Mindin–αM-Integrin endocytosis activates STAT3 to maintain keratinocyte stemness

Binita Dam[1,2,3], Johan Ajnabi[1,2], Tirthankar Saha[1], Krithika Badarinathan[1] , Akshay Hegde[1], Abhik Dutta[1,4], Siddham Jasoria[1], Sunny Kataria[1] and Colin Jamora[1,3,*]

1.Institute for Stem Cell Science and Regenerative Medicine (inStem), Bangalore 560065, India

2.Manipal Academy of Higher Education (MAHE), Manipal 576104, India

3. Department of Life Sciences, Shiv Nadar Institution of Eminence, Delhi-NCR, India

4.School of Chemical and Biotechnology, Shanmugha Arts, Science, Technology and Research Academy (SASTRA) University, Thanjavur, Tamil Nadu 613401, India

*Corresponding author: Colin Jamora

Department of Life Sciences, Shiv Nadar Institution of Eminence

NH91, Tehsil Dadri, Greater Noida, Uttar Pradesh – 201314, India

Phone: 7011115898

Email: colin.jamora@snu.edu.in

Abstract

Keratinocyte stem cell fate in skin regeneration and carcinomas is orchestrated by a complex integration of niche signals and intracellular signalling cascades. However, the subcellular organization and dynamic regulation of these pathways remain poorly understood. Here, we uncover the intracellular signalling mechanism initiated by the interaction between the extracellular matrix protein Mindin and αM-integrin receptor (CD11b), leading to activation of the transcription factor STAT3, a key regulator of keratinocyte stemness. We have found that the F-Spondin domain of Mindin is the minimal region required for integrin engagement and downstream signalling. This interaction promotes endocytosis of the Mindin–CD11b complex into early endosomes, which in turn activates STAT3. Notably, we found that the non-receptor tyrosine kinase Src regulates this endocytosis, revealing a previously undefined route of STAT3 activation. Finally, we demonstrate the functional requirement of this Mindin–CD11b endocytosis–driven STAT3 signalling in maintaining stemness in a keratinocyte cancer stem cell model. These findings illuminate a subcellular mechanism by which Mindin-integrin signalling regulates keratinocyte stemness.

Introduction

The balance between self-renewal and differentiation of keratinocyte stem cells dictates whether the epidermis maintains homeostasis, initiates wound repair or progresses toward carcinoma development(*1*). The context dependent fate changes in these cells are largely dependent on the signalling factors in the niche and their integration into specific intracellular events(*2*). Signal Transducer and Activator of Transcription 3(STAT3), a member of the STAT family of transcription factors, emerges as a pivotal intracellular effector in keratinocyte stem cell regulation. It supports the proliferation and survival of keratinocyte stem cells residing in the basal layer of the epidermis. Evidence from keratinocyte-specific STAT3 knockout models has demonstrated that loss of STAT3 impairs skin regeneration due to defective cell proliferation and migration. Conversely, constitutive activation of STAT3 signalling is commonly observed in various skin cancers. Cytokines like, Interleukin-6 (IL-6) and Interleukin-22 (IL-22) and Epidermal Growth Factor (EGF) have been reported to drive STAT3 activation in skin regeneration or pathogenesis (*3–5)*. Given its prominent role in oncogenesis, especially in epithelial cancers, STAT3 activation has been the target of multiple therapeutic strategies. Although some of these strategies have shown promise in preclinical models and early clinical trials, they have largely failed in later-phase studies, primarily due to either toxicity or lack of efficacy(*3–5*). The toxicity is likely due to the essential role of canonical STAT3 signalling in maintaining normal tissue homeostasis. Meanwhile, treatment inefficacy may be attributed to compensatory activation of STAT3 through non-canonical pathways that bypass the usual regulatory mechanisms. This has led to renewed interest in identifying novel, targetable STAT3 regulators driving skin carcinomas.

In our recent work using a murine model of skin carcinoma, we identified Mindin (Spondin-2), a soluble matricellular protein, as novel, non-canonical regulator of STAT3 activation in basal proliferating keratinocytes. Mindin mediated STAT3 activation functions to maintain the stem/progenitor state of keratinocytes. Mindin activates STAT3 through its interaction with leukocyte specific αM-integrin (CD11b) expressed on the surface of keratinocytes followed by subsequent activation of a non-receptor tyrosine kinase Src. Disruption of this interaction abrogates the activation of the STAT3 pathway and keratinocytes lose their stemness characteristics. Likewise, perturbation of this pathway along any of its components decreases the cancer stem cell population and limits the tumorgenicity of human squamous cell carcinoma cells(*6*).

However, the precise mechanism by which the Mindin–integrin interaction at the plasma membrane is translated into intracellular activation of Src and STAT3 remains unknown. It is now well recognized that signal transduction is not merely a linear cascade but a process intricately shaped by the spatial and temporal dynamics of molecular interactions(*7*, *8*). These dynamics govern the strength, duration, and compartmental specificity of signalling events, ultimately dictating complex outcomes such as stemness. Unravelling how Mindin orchestrates the spatiotemporal activation of Src-STAT3 signalling will help define discrete intracellular hubs and regulatory checkpoints that control keratinocyte stem cell fate.

Results

F-Spondin domain of Mindin is the minimal domain to activate STAT3 in keratinocytes

To probe the mechanism by which Mindin activates STAT3 in a CD11b dependent manner, we first focused on characterising the specifics of the ligand-receptor interaction. Ligand-receptor interactions are mediated by specific segments in the ligand and receptor which are defined as minimal domains. They are necessary and sufficient to mediate binding and signal transduction. Mindin contains two main domains: F-Spondin and Thrombospondin (TSP-1)(*9*, *10*). The association of integrins to their ligands is critically dependent on metal ion-dependent adhesion sites (MIDAS) within the integrin and ligand molecules. Structural analysis of Mindin revealed that F-Spondin domain of Mindin contains amino acid residues that can coordinate to bind metal ions, suggesting potential interaction with integrins(*9*). Hence, we investigated the interaction of F-Spondin domain of Mindin with CD11b. Co-Immunoprecipitation of CD11b from keratinocytes treated with purified recombinant F-Spondin showed that CD11b binds to F-Spondin (Fig.1A). We further evaluated if the interaction between F-Spondin and CD11b on keratinocytes is MIDAS dependent. Among the putative MIDAS-forming amino acid residues, glutamate at position 115 in the F-Spondin domain is conserved and present in known integrin ligands such as ICAM-1. We generated a point mutant wherein Glutamate residue at 115 was changed to Alanine [F-Spondin(E115A)]. Co-Immunoprecipitation of CD11b from keratinocytes treated with purified recombinant F-Spondin(E115A) analysis showed that CD11b failed to bind to the [F-Spondin(E115A)] mutant (Fig.1A). We then investigated if F-Spondin domain is sufficient to activate STAT3. We observed that F-Spondin treatment resulted in elevated levels of pSTAT3 compared to buffer control treatment and the increase is comparable to that elicited by the treatment with full length Mindin (Fig.1B). We further verified if STAT3 activation in keratinocytes is dependent on F-Spondin-CD11b interaction. For this, we treated WT keratinocytes with F-Spondin[E115A] that fails to bind to CD11b and CD11b blocking antibody. Perturbation of F-Spondin-CD11b interaction failed to mediate STAT3 activation (Fig.1C and 1D). Hence, F-Spondin domain of Mindin is the minimal domain sufficient to interact to CD11b and activate STAT3 in mouse keratinocytes.

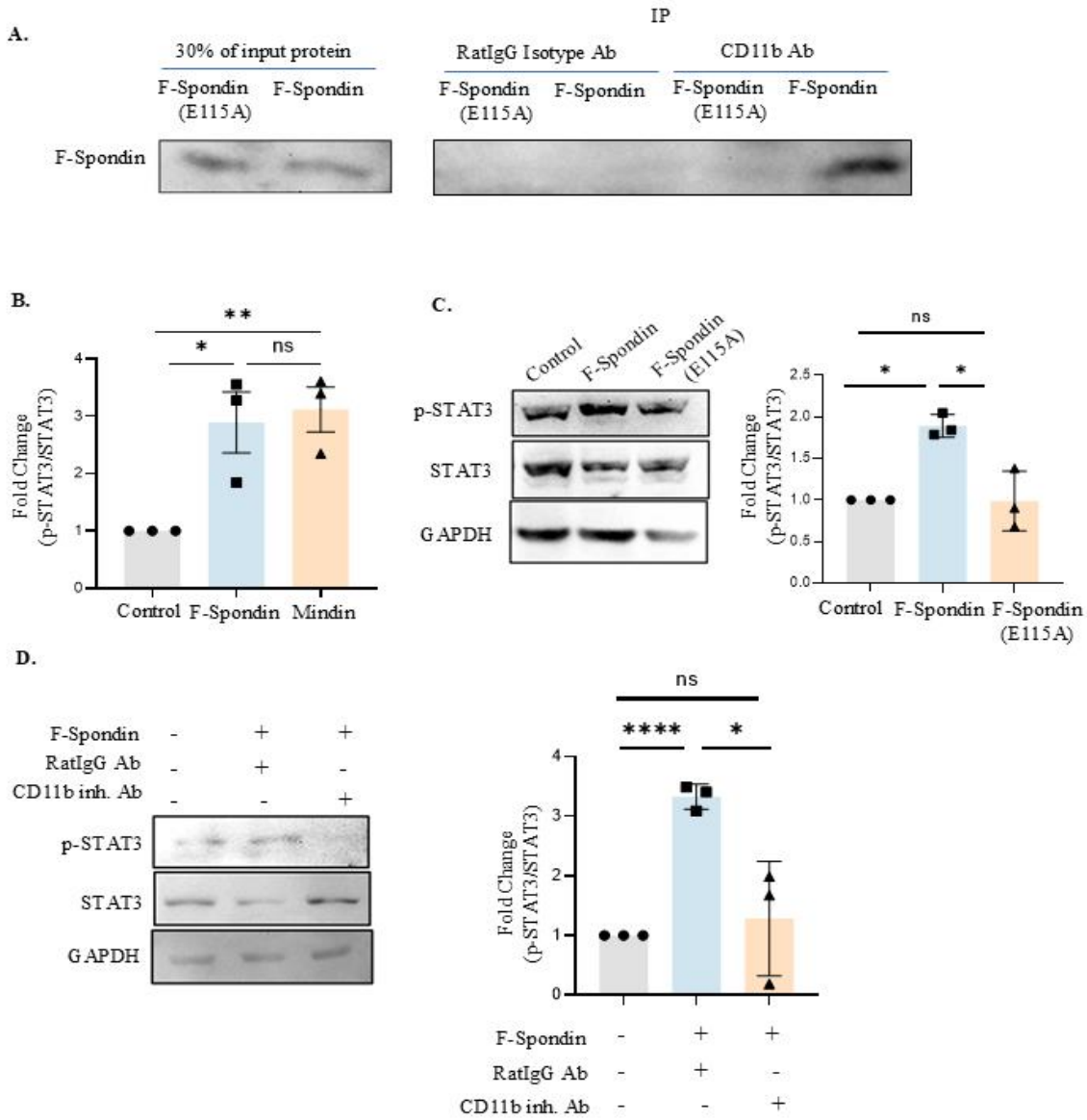

Fig.1. F-Spondin domain of Mindin interacts with CD11b and activates STAT3 in primary mouse keratinocytes. (A) Co-immunoprecipitation of F-Spondin with CD11b from keratinocytes treated with either recombinant wild-type F-Spondin or F-Spondin mutant (FSE115A). Immunoprecipitated F-Spondin was detected by immunoblotting (Representative image among n=3 independent experiments)**. (B)** Quantification of phosphorylated STAT3 (p-STAT3) levels relative to total STAT3(represented as fold change) in keratinocytes treated with recombinant

Mindin or F-Spondin. (n=3). **(C)** Left: Immunoblot and Right: densitometric quantification of p-STAT3 levels relative to total STAT3 in keratinocytes treated with recombinant wild-type F-Spondin or F-Spondin mutant (FSE115A) (n=3). **(D)** Left: Immunoblot and Right: densitometric quantification of p-STAT3 levels relative to total STAT3 in keratinocytes treated with F-Spondin in the presence or absence of a CD11b-blocking antibody (n=3). (Data represent the mean ± SEM. p values were calculated using student's t-test. *$p < 0.05$ and **$p < 0.01$ and ns = not significant.)

F-Spondin domain is sufficient to maintain stemness in keratinocytes

Our past work has revealed that STAT3 activation upon Mindin-CD11b interaction leads to stemness maintenance in keratinocytes(*6*). Hence, we evaluated if F-Spondin domain is also sufficient to mediate stemness in keratinocytes. We began to assess the stemness signature at the global gene expression level with bulk RNA sequencing and compared the transcriptome profile of Mindin treated keratinocytes to that of F-Spondin treated keratinocytes. The transcriptome analysis of F-Spondin treated keratinocytes revealed that almost 80% (237 out of 331, Fig.) of differentially expressed genes (adjusted $P < 0.05$, $\log_2$ fold change ≥ 1, or $\log_2$ fold change ≤ 1) overlap with that of Mindin treated keratinocytes (Fig.2A). Intriguingly, Gene Ontology of these overlapping genes exhibited significant fold enrichment of biological process like, cell proliferation and differentiation pathways (Fig.2B). qPCR analysis validated that proliferation (*CyclinD1*), survival (*Myc*) and keratinocyte specific stemness genes (*Sox4, Igfir*) (Fig.2C) were upregulated in Mindin and F-Spondin treated keratinocytes. Thus, the gene expression analysis suggests that F-Spondin domain of Mindin is sufficient to regulate stemness associated genes and processes in primary mouse keratinocytes. We further investigated whether F-Spondin is also sufficient to enhance the stem/progenitor characteristics in WT keratinocytes. We observed that F-Spondin treated keratinocytes exhibited an increased nuclear to cytoplasmic ratio (Fig.2D and E), colony-forming capacity (Fig.2F) and expression of CD44, a cell surface marker for stemness(*6*) (Fig.2G). In summary, we found that the F-Spondin domain of Mindin is sufficient to maintain the stemness properties of epidermal keratinocytes.

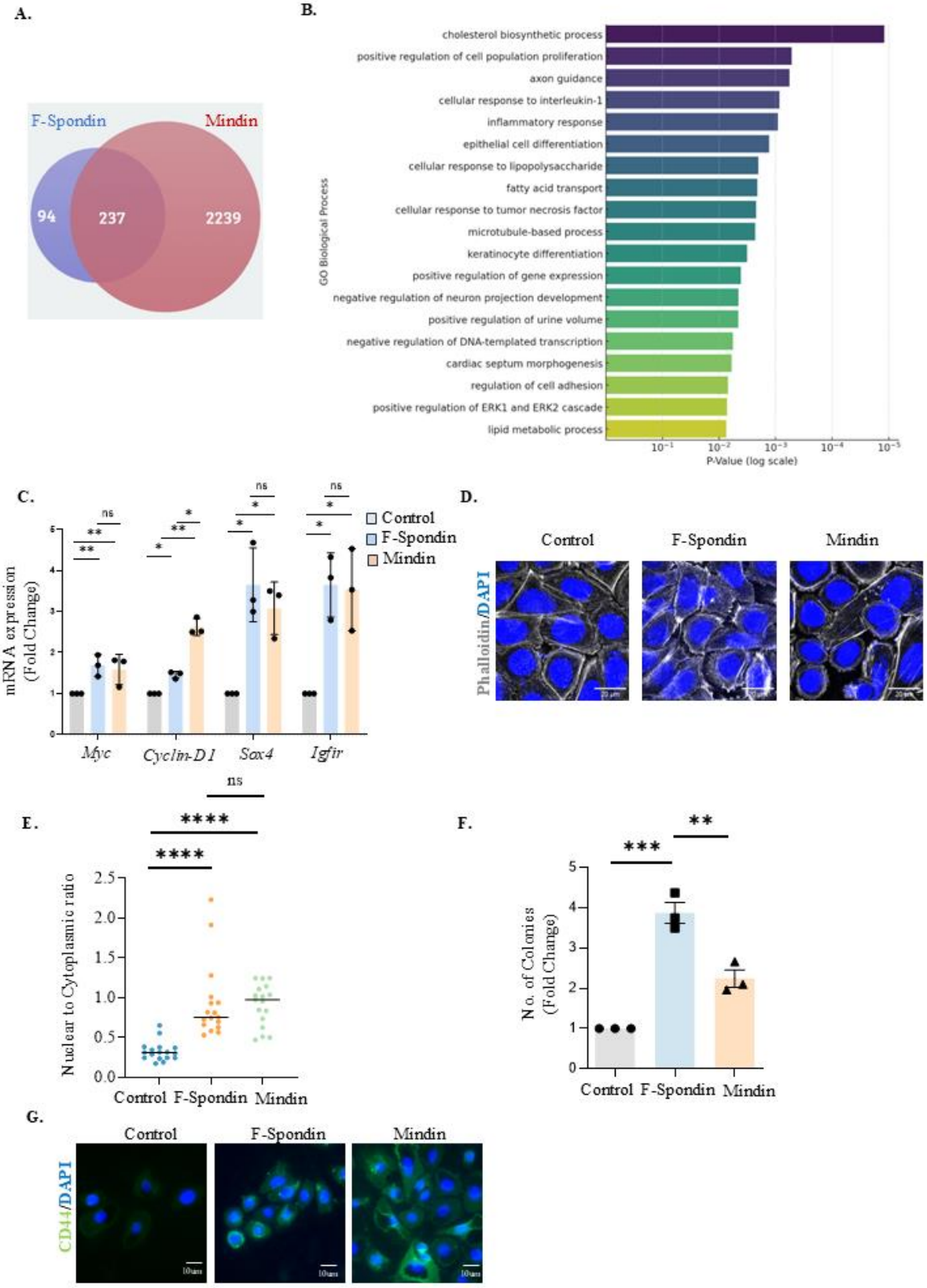
A.
F-Spondin
Mindin
94
237
2239
B.
cholesterol biosynthetic process
positive regulation of cell population proliferation
axon guidance
cellular response to interleukin-1
inflammatory response
epithelial cell differentiation
cellular response to lipopolysaccharide
fatty acid transport
cellular response to tumor necrosis factor
microtubule-based process
keratinocyte differentiation
positive regulation of gene expression
negative regulation of neuron projection development
positive regulation of urine volume
negative regulation of DNA-templated transcription
cardiac septum morphogenesis
regulation of cell adhesion
positive regulation of ERK1 and ERK2 cascade
lipid metabolic process
GO Biological Process
P-Value (log scale)
C.
mRNA expression (Fold Change)
Control
F-Spondin
Mindin
Myc
Cyclin-D1
Sox4
Igfir
D.
Control
F-Spondin
Mindin
Phalloidin/DAPI
E.
Nuclear to Cytoplasmic ratio
Control
F-Spondin
Mindin
F.
No. of Colonies (Fold Change)
Control
F-Spondin
Mindin
G.
Control
F-Spondin
Mindin
CD44/DAPI

Fig. 2. F-Spondin domain is sufficient to maintain stemness in keratinocytes. (A) Venn diagram of overlapping differentially regulated genes in Mindin-treated mouse keratinocytes and F-Spondin treated mouse keratinocytes (adjusted $P < 0.1$, $\log_2$ fold change >1, or $\log_2$ fold change ≤ 1). **(B)** Significant biological processes of GOTERMS of differentially regulated genes common in Mindin-treated keratinocytes and F-Spondin treated keratinocytes (Fold enrichment= $-\log_{10}$padj, padj<0.05) **(C)** qPCR data of proliferation (*Cyclin D1*), survival (*Myc*) and keratinocyte specific stemness associated genes (*Sox4, Igfir*). Represented as fold change (n=3). **(D)** Immunofluorescence images of keratinocytes stained for phalloidin (marking actin demarcating cell boundary) and Hoechst (marking cell nucleus) under control, F-Spondin and Mindin treatment. **(E)** Quantification of nuclear to cytoplasmic ratio from phalloidin and Hoechst-stained immunofluorescence images of keratinocytes as represented in (D) (Individual cells counted from n=3 independent experiments). **(F)** Number of colonies formed by keratinocytes in control vs F-Spondin and Mindin treated keratinocytes (Represented as fold change, n=3). **(G)** Immunofluorescence images of keratinocytes stained with keratinocyte stem cell marker, CD44(in green) in control, F-Spondin and Mindin treated conditions. Hoechst marks the nucleus. (C, E, F) Data represent the mean ± SEM. p values calculated using student's t-test. *p < 0.05 and **p < 0.01 and ns = not significant.

F-Spondin mediates endosomal trafficking of CD11b to activate STAT3 and maintain keratinocyte Stemness

We next investigated the mechanism by which the engagement F-Spondin with CD11b at the cell surface results in the intracellular activation of a transcription factor. Signaling can occur at both the cell surface (EGF signaling) or upon internalization of the ligand-receptor complex (such as TGFb) (*11*). Our data revealed that, the percentage of cells expressing surface CD11b was reduced upon F-Spondin treatment as detected by flow cytometric analysis (Fig.3B). However, the total CD11b protein levels are the same under both conditions (Fig.3A). This suggests that CD11b undergoes internalisation upon F-Spondin treatment. Receptor internalization in cells occurs via endocytic pathways mediated by cytoplasmic vesicles known as endosomes(ref). Hence, we investigated whether CD11b is redistributed to the endosome upon treatment with F-Spondin. We observed that F-Spondin treatment induced the colocalization of CD11b with the early endosome (marked by EEA) (Fig.3C and 3D) and the colocalization is lost upon CD11b inhibitory antibody

treatment (Fig.3C and 3D). Receptor mediated endocytosis is majorly routed through clathrin dependent endocytosis mechanism. To further validate F-Spondin mediated CD11b endocytosis, we utilised “dynasore”, an inhibitor that inactivates dynamin, which is essential for the clathrin dependent pathway. Flow cytometry analysis to quantify the surface expression of CD11b revealed that, exposure of F-spondin treated cells to dynasore inhibited the endocytosis of CD11b(Fig.3E). These data suggests that F-Spondin induces CD11b internalisation via the Clathrin mediated endocytic pathway.

We further tested whether the F-Spondin mediated activation of STAT3 is dependent on endocytosis of the CD11b receptor. Cells treated with F-spondin in the presence of dynasore failed to activate the STAT3 pathway as indicated by the p-STAT3 levels which was comparable to buffer treated cells (Fig.3F). We also check if the enhanced stemness properties in keratinocytes by F-Spondin is altered by blocking endocytosis. The increase in nuclear to cytoplasmic ratio mediated by F-Spondin was prevented upon blocking endocytosis (Fig.3G). Similarly, we did not observe CD44 expression in keratinocytes treated with dynasore (Fig.3H). Altogether, these data reveal that the F-Spondin mediated CD11b endocytosis is necessary for STAT3 activation and associated stemness in keratinocytes.

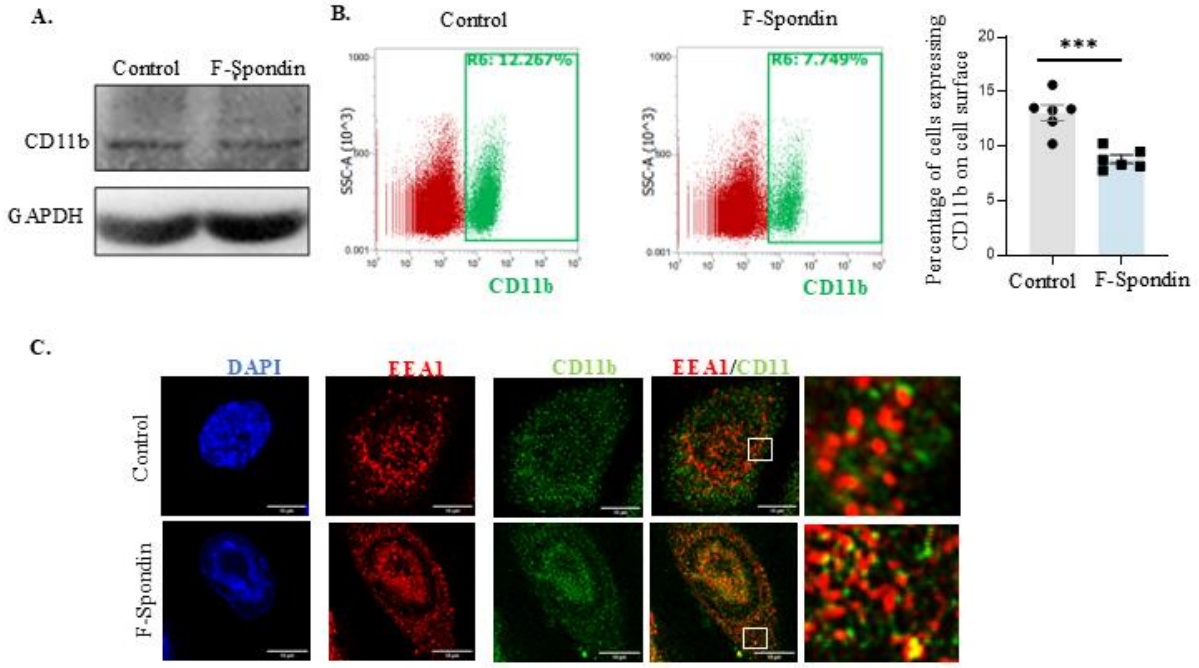

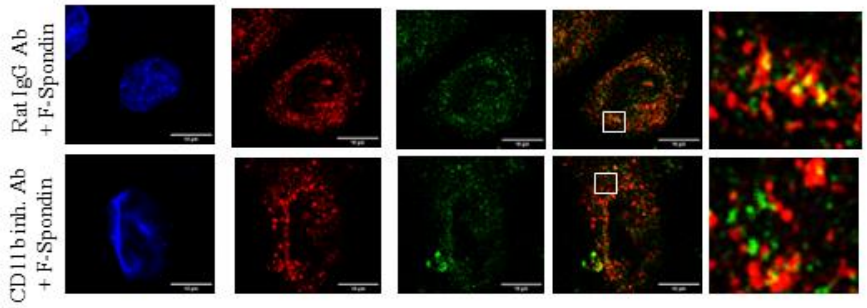
Rat IgG Ab
+ F-Spondin
CD11b inh. Ab
+ F-Spondin

D.

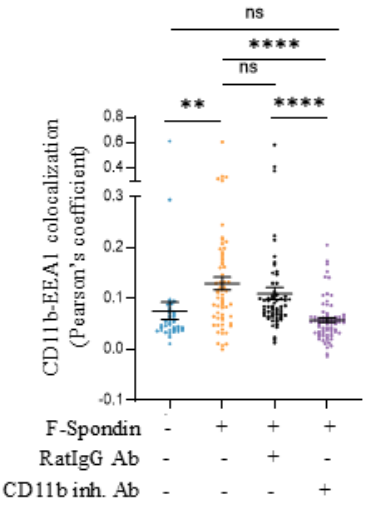
ns
****
ns
**
****
CD11b-EEA1 colocalization
(Pearson's coefficient)
F-Spondin - + + +
RatIgG Ab - - + -
CD11b inh. Ab - - - +

E.

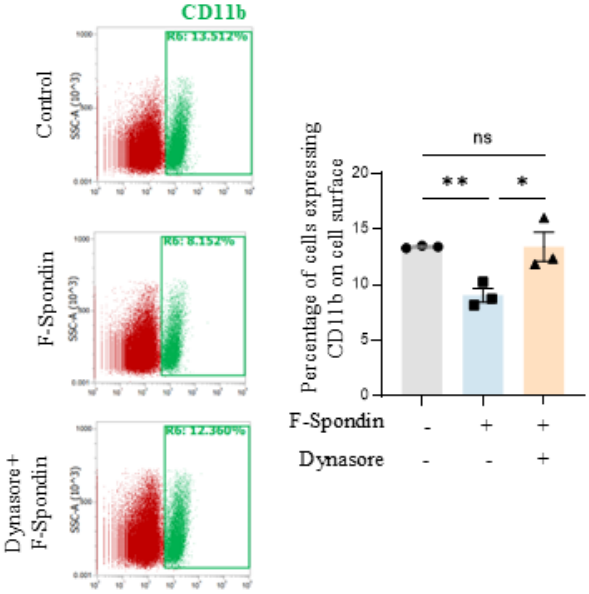
CD11b
Control
F-Spondin
Dynasore+
F-Spondin
R6: 13.512%
R6: 8.152%
R6: 12.360%
Percentage of cells expressing
CD11b on cell surface
ns
**
*
F-Spondin - + +
Dynasore - - +

F.

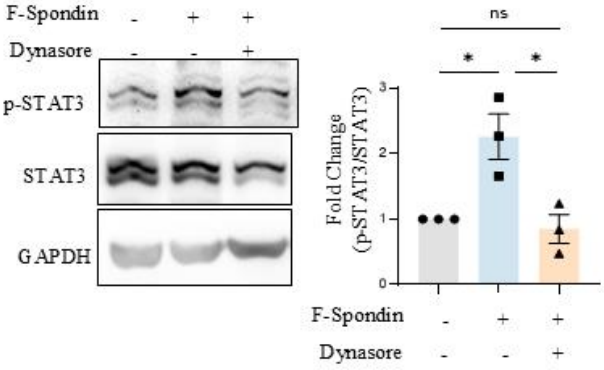
F-Spondin - + +
Dynasore - - +
p-STAT3
STAT3
GAPDH
ns
*
*
Fold Change
(p-STAT3/STAT3)
F-Spondin - + +
Dynasore - - +

G.

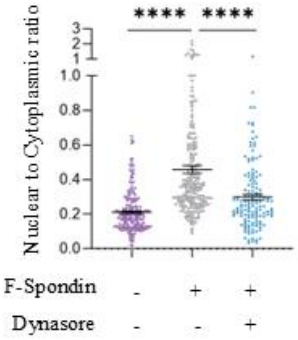
****
****
Nuclear to Cytoplasmic ratio
F-Spondin - + +
Dynasore - - +

H.

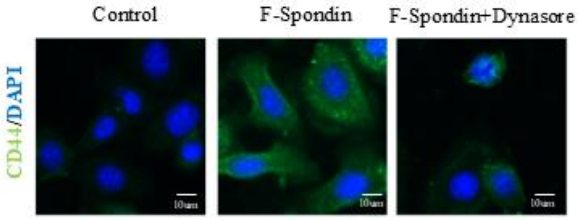
Control
F-Spondin
F-Spondin+Dynasore
CD44/DAPI

Fig. 3. F-Spondin mediated endocytosis of CD11b is necessary for STAT3 activation and stemness in primary mouse keratinocytes (A) Immunoblot of CD11b and GAPDH (internal control) in control and F-Spondin treated keratinocytes. **(B)** Left: Flow cytometry data showing percentage of cells with surface CD11b levels in control and F-Spondin treated keratinocytes. Right: Quantification, n=6. **(C)** Immunofluorescence images showing colocalisation of EEA1(endosomal marker, in red) and CD11b (in green) in control, F-Spondin, Rat IgG +F-Spondin, or CD11b inhibitory Ab +F-Spondin treated keratinocytes. Hoechst marks the cell nucleus. Images are represented from single mid-optical section. **(D)** Quantification of colocalization of CD11b and EEA1 per cell in form of Pearson's correlation coefficient, n=50-80 cells from three independent experiments). **(E)** Left: Flow cytometry data showing percentage of cells with surface CD11b levels in control, F-Spondin and dynasore+F-Spondin treated keratinocytes. Right: Quantification, n=3. **(F)** Left: Representative immunoblot of p-STAT3, STAT3 and GAPDH (internal control) in control, F-Spondin and dynasore+F-Spondin treated keratinocytes. Right: Quantification of p-STAT3/STAT3 levels from immunoblot, n=3. **(G)** Quantification of Nuclear to cytoplasmic ratio in control, F-Spondin and dynasore+F-Spondin treated keratinocytes, n=80-100 cells from three independent experiments. **(H)** Immunofluorescence images of keratinocytes stained with keratinocyte stem cell marker, CD44(in green) in control, F-Spondin and Mindin treated conditions. Hoechst marks the nucleus. Data represents the mean ± SEM. p values calculated using student's t-test (B, E, F, G) and Kruskal-Wallis Test(D). *$p < 0.05$, **$p < 0.01$, ***$p < 0.001$ and ****$p < 0.0001$ and ns = not significant

F-Spondin mediated endocytosis of CD11b is dependent on Src kinase activation

We next investigated the mechanism of the recruitment of the endocytic machinery upon F-Spondin-CD11b interaction. As per our previous study, Mindin-CD11b interaction activates Src kinase which is obligatory for downstream STAT3 activation in keratinocytes(*6*). Moreover, ligand-receptor interaction mediated Src kinase activation has been reported to be involved in regulating clathrin-mediated endocytosis(*12*, *13*). We observed increased levels of p-Src upon F-Spondin treatment (Fig.4A) in keratinocytes and blocking its activity by Src kinase activity inhibitor led to failure in STAT3 activation (Fig.4B). We evaluated if Src activation lies upstream to endocytosis and controls the process. Flow cytometry analysis revealed that inhibition of Src activity led to failure in the internalisation of CD11b upon F-Spondin treatment (Fig.4C).

Similarly, colocalization of CD11b in early endosomes was also blocked upon Src kinase activity inhibition (Fig.4D). In summary, the results suggest F-Spondin-CD11b interaction is followed by Src kinase activation which further induces endocytosis of the complex and leads to STAT3 activation. We have further confirmed the necessity of Src kinase activity with respect to maintenance of stemness properties by F-Spondin. F-Spondin mediated higher nuclear to cytoplasmic ratio and CD44 expression was reversed upon blocking Src activity (Fig.4E and 4F).

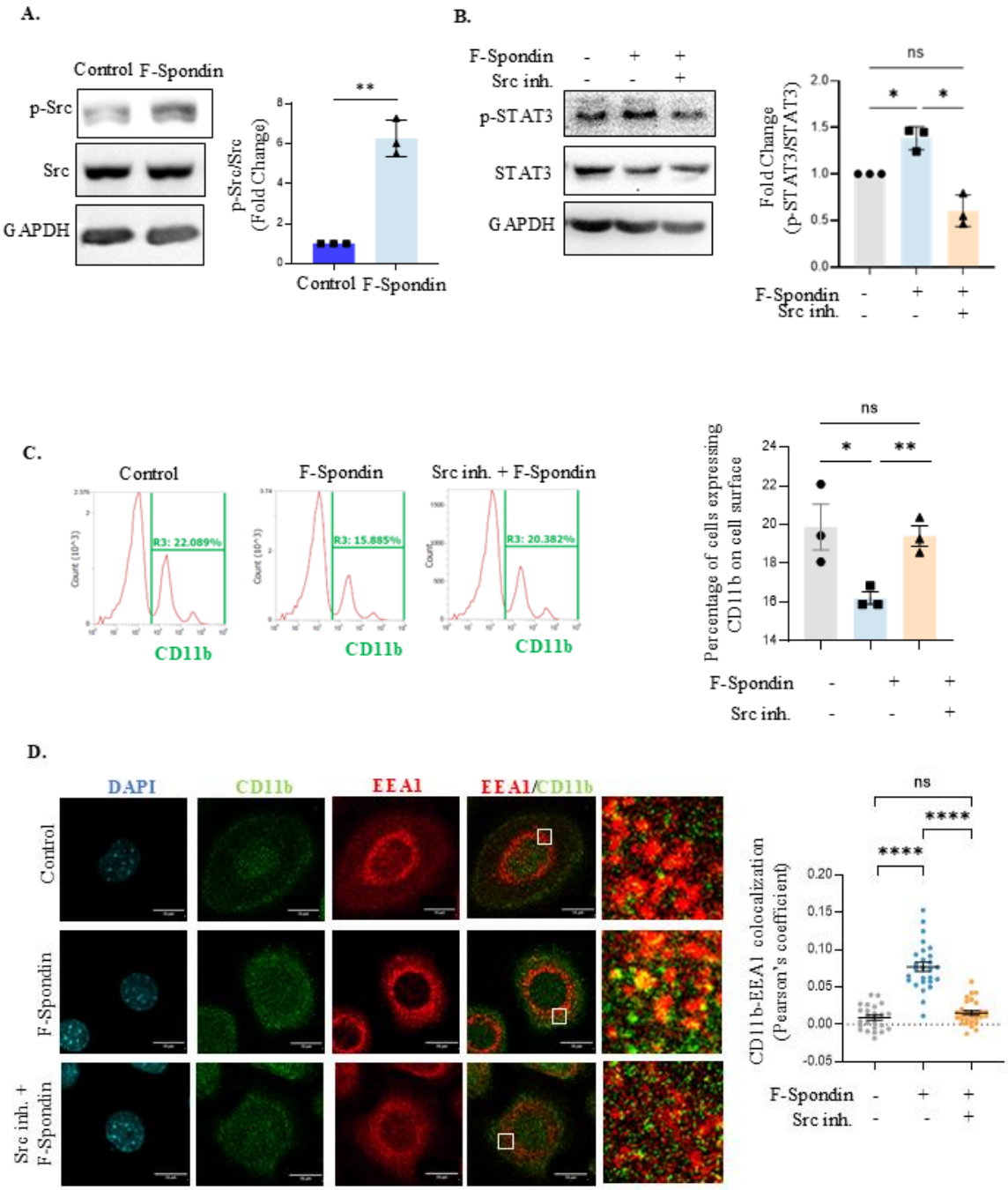

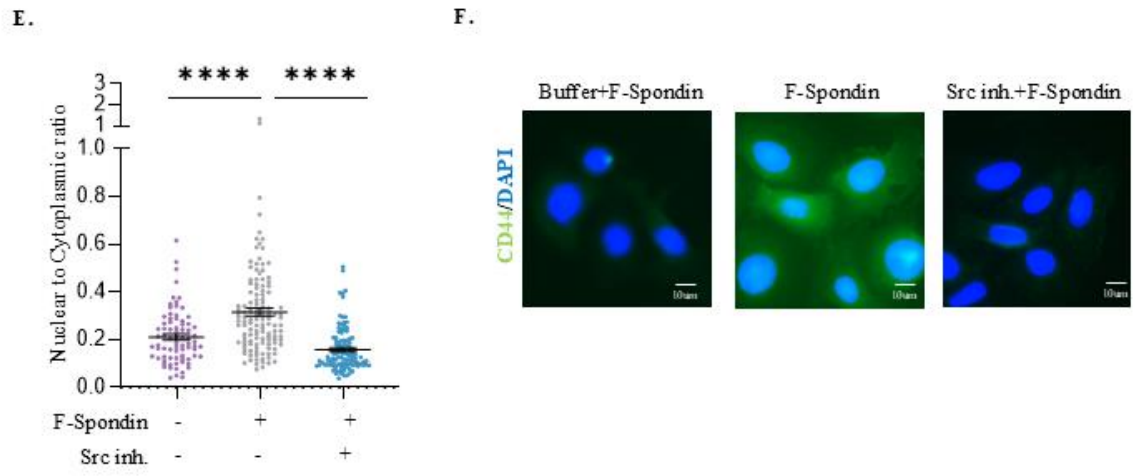

Fig. 4. Endocytosis of CD11b is dependent upon Src kinase activity. (A) Left: Representative immunoblot of p-Src, Src and GAPDH (internal control) in control and F-Spondin treated keratinocytes. Right: Quantification of p-Src/Src levels from immunoblot, n=3. **(B)** Left: Representative immunoblot of p-STAT3, STAT3 and GAPDH (internal control) in control, F-Spondin and Src inhibitor+F-Spondin treated keratinocytes. Right: Quantification of p-STAT3/STAT3 levels from immunoblot, n=3. **(C)** Left: Flow cytometry data showing percentage of cells with surface CD11b levels in control, F-Spondin and Src inhibitor+F-Spondin treated keratinocytes. Right: Quantification, n=3. **(D)** Immunofluorescence images showing colocalisation of EEA1(endosomal marker, in red) and CD11b (in green) in control, F-Spondin and Src inhibitor+F-Spondin treated keratinocytes. Hoechst marks the cell nucleus. Images are represented from single mid-optical section. **(D)** Quantification of colocalization of CD11b and EEA1 per cell in form of Pearson's correlation coefficient (n=20-30 cells from three independent experiments). **(E)** Quantification of Nuclear to cytoplasmic ratio in control, F-Spondin and Src inhibitor + F-Spondin treated keratinocytes, n=80-100 cells from three independent experiments. **(F)** Immunofluorescence images of keratinocytes stained with keratinocyte stem cell marker, CD44 (in green). Hoechst marks the cell nucleus. Data represent the mean ± SEM. p values calculated using student's t-test (A-C, E) and Kruskal-Wallis test(D), *$p < 0.05$, **$p < 0.01$, ***$p < 0.001$ and ****$p < 0.0001$ and ns = not significant.

CD11b endocytosis is necessary for stemness maintenance in epidermal cancer model

STAT3 is known to be hyperactivated in a variety of cancers(*14*, *15*). Similarly, Mindin has been reported to be overexpressed in malignancies such as prostate cancer, where it also serves as a diagnostic biomarker(*16*). The direct regulation of STAT3 activity by Mindin was first reported in our previous work in a murine model in which the transcription factor Snail is overexpressed in basal proliferative keratinocytes. Mindin mediated STAT3 activation in Snail-transgenic keratinocytes leads to sustained stemness characteristics in these cells, driving epidermal hyperplasia and creating a tumour conducive microenvironment(*6*). We investigated whether Mindin-dependent STAT3 activation in Snail transgenic keratinocytes requires CD11b receptor endocytosis as a mechanistic step. Flow cytometric analysis revealed reduction in the percentage of cells expressing surface CD11b in Snail transgenic keratinocytes as compared to the WT keratinocytes (Fig.5A). Further, blocking endocytosis by dynasore treatment on cells, led to failure in the reduction of CD11b surface levels in Snail transgenic keratinocytes (Fig.5A). Next, we verified if STAT3 activation in Snail transgenic keratinocytes is dependent on endocytosis. Western blot data revealed that the p-STAT3/STAT3 level which is upregulated in Snail transgenic keratinocytes is lost upon blocking endocytosis by dynasore (Fig.5B). We also observed significantly higher CD11b-EEA1 colocalization in Snail transgenic keratinocytes which is reduced upon CD11b receptor blocking (Fig.5C). These results suggest that regulation of STAT3 signalling in keratinocyte stem cell model driving epidermal carcinoma is dependent on ligand-receptor mediated endocytosis process. As reported previously, STAT3 activation in Snail transgenic keratinocytes enhances the stemness properties of these cells. Hence, we evaluated if receptor mediated endocytosis is necessary for regulating stemness behaviour in these cells. Increase in nuclear to cytoplasmic ratio observed in the cells is reduced upon dynasore treatment (Fig.5E). Higher CD44 expression that is observed in Snail transgenic keratinocytes as compared to WT keratinocytes is also reduced in dynasore treated condition (Fig.5F).

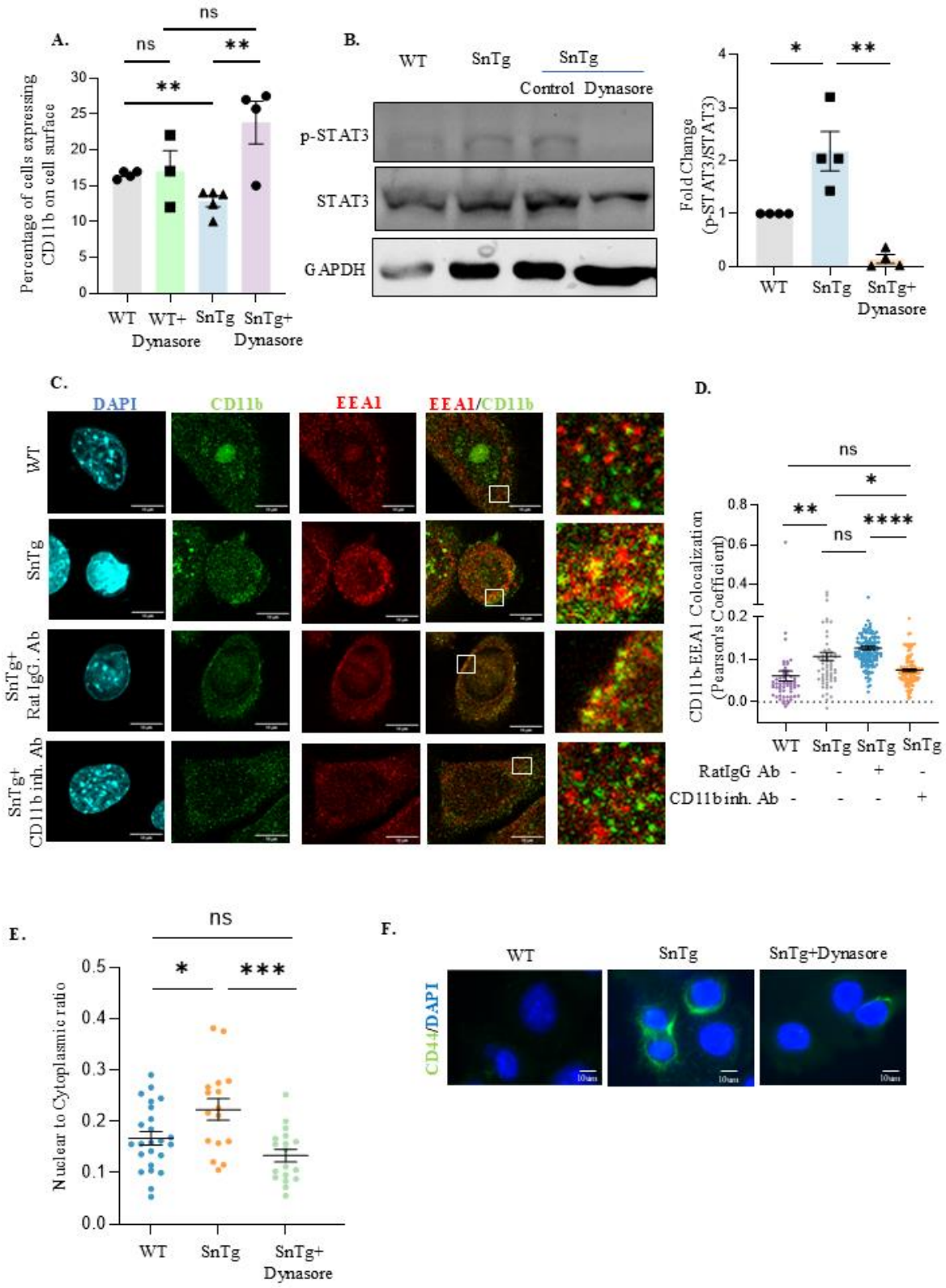
A.
ns
ns
**
**
Percentage of cells expressing CD11b on cell surface
30
25
20
15
10
5
0
WT
WT+ Dynasore
SnTg
SnTg+ Dynasore
B.
WT
SnTg
SnTg
Control
Dynasore
p-STAT3
STAT3
GAPDH
*
**
Fold Change (p-STAT3/STAT3)
4
3
2
1
0
WT
SnTg
SnTg+ Dynasore
C.
DAPI
CD11b
EEA1
EEA1/CD11b
WT
SnTg
SnTg+ RatIgG. Ab
SnTg+ CD11b inh. Ab
D.
ns
*
**
ns
****
CD11b-EEA1 Colocalization (Pearson's Coefficient)
0.8
0.6
0.4
0.2
0.1
0.0
WT
SnTg
SnTg
SnTg
RatIgG Ab - - + -
CD11b inh. Ab - - - +
E.
ns
*
***
Nuclear to Cytoplasmic ratio
0.5
0.4
0.3
0.2
0.1
0.0
WT
SnTg
SnTg+ Dynasore
F.
WT
SnTg
SnTg+Dynasore
CD44/DAPI

Fig. 5. CD11b Endocytosis in epidermal cancer model. (A) Quantification of percentage of cells expressing CD11b surface levels in wild type (WT) primary mouse keratinocytes +/- dynasore and Snail transgenic (SnTg) mouse keratinocytes +/- dynasore. **(B)** Left: Representative immunoblot of p-STAT3, STAT3 and GAPDH (internal control) in WT and SnTg keratinocytes and SnTg keratinocytes+/- dynasore. Right: Quantification of p-STAT3/STAT3 levels from immunoblot, n=3. **(C)** Representative immunofluorescence images of CD11b (in green)-EEA1(in red) colocalisation in WT and SnTg keratinocytes and SnTg treated with RatIgG Ab and Cd11b inhibitory Ab. Hoechst marks the nucleus. Images are represented from single mid-optical section. **(D)** Quantification of colocalization of CD11b and EEA1 per cell in form of Pearson's correlation coefficient, n=80-100 cells from three independent experiments. (E) Quantification of Nuclear to cytoplasmic ratio in WT and SnTg keratinocytes +/- dynasore, n=30-40 cells from three independent experiments. **(F)** Immunofluorescence images of keratinocytes stained with keratinocyte stem cell marker, CD44 (in green). Hoechst marks the cell nucleus. Data represents the mean ± SEM. p values calculated using student's t-test (A, B, E) and Kruskal-Wallis Test(D), *$p < 0.05$, **$p < 0.01$, ***$p < 0.001$ and ****$p < 0.0001$ and ns = not significant.

Discussion

How distinct signalling proteins in a pathway coordinate seamlessly across cellular space and time to govern complex cellular behaviours has always been an intriguing puzzle. Our findings reveal a spatially defined mechanism in which the extracellular matrix protein Mindin engages an integrin, a tyrosine kinase, and a key transcription factor to preserve keratinocyte stem cell fate.

We identify the F-Spondin domain as the minimal domain of Mindin for engaging αM-integrin (CD11b) in keratinocytes via metal-ion dependent interaction site. This domain has previously been shown to bind CD11b in macrophages and promote its activation, suggesting that the Mindin–CD11b interaction interface is conserved across different cell types(*10*). Interestingly, sequence alignment has shown that Leucine, Glutamate and Valine amino residues which forms metal ion binding pocket in F-spondin of Mindin and cardinal to CD11b binding, is not conserved among other F-Spondin domain in the protein family(*9*). This provides CD11b binding specificity to Mindin compared to other known Mindin-FS family proteins. It would be interesting to understand how Mindin–CD11b binding alters integrin conformation to trigger downstream signalling.

Upon ligand binding, integrins get activated and known to undergo regulated endocytosis that controls their surface availability and this trafficking influences processes such as migration and invasion(*17–19*). Here we show F-Spondin mediated spatial relocation of CD11b from the plasma membrane to endosomal compartments establishes a signalling environment conducive to STAT3 activation. This requirement reframes CD11b not simply as a surface-bound adhesion receptor but as a trafficking-dependent signalling hub.

There are reports which have shown that endosomes serve as active signalling platforms for sustained STAT3 activation mediated by cytokines(*20*, *21*). Cytokine driven endosomal STAT3 activation has been reported to play critical role in stemness programs in embryonic and haematopoietic stem cells(*22*). By showing that endocytosis is essential for STAT3 activation and keratinocyte stemness maintenance, our findings underscore the broader importance of endocytosis as a regulatory mechanism that shapes critical signalling nodes governing cell fate decisions. However, the factors that dictate whether STAT3 is activated at endosomes rather than at the plasma membrane remain to be elucidated.

We report that Src serves as the molecular bridge between integrin internalization and activation of transcriptional stemness programs. This is supported by reports that members of Src family kinases can interact with and phosphorylate components of the endocytic machinery, including

clathrin and epsin(*13*, *23*, *24*). These interactions play a critical role in promoting the assembly of clathrin, a key step in the initiation of clathrin-mediated endocytosis.

The demonstration that blocking CD11b endocytosis disrupts STAT3 activation and depletes cancer stem cell populations underscores the functional necessity of this pathway in tumor maintenance. Endocytosis is increasingly recognized as a key regulator of oncogenic signalling by controlling receptor availability, signal duration, and subcellular localization(*25*). For example, dysregulated integrin endocytosis promotes invasive behavior in breast cancer cells(*26*), while altered EGFR trafficking sustains proliferative signalling in glioblastoma(*27*). Furthermore, Dynamin inhibitors such as Dynasore, MiTMAB, and Dynole-34-2 have demonstrated potent anti-proliferative and pro-apoptotic effects in cervical cancer and other tumour cell lines, suggesting their potential as adjunct agents in combination treatments(*28*).

By elucidating the mechanism from Mindin engagement to Src-dependent STAT3 activation, our study establishes a new paradigm in epidermal carcinoma stem cell regulation in which extracellular matrix ligand co-opts integrin trafficking to spatially organize intracellular signalling. These results extend the concept of “endomembrane signalling” to integrin biology, reinforcing that ligand-induced endocytic trafficking is not merely a receptor turnover process but a spatial switch that modulates signal quality and transcriptional outcome.

Targeting the F-Spondin–CD11b interaction surface, or its associated endocytic machinery, could selectively dismantle the stemness-supporting niche without broadly impairing integrin functions essential for tissue homeostasis.

Materials and Methods

Cell Culture

Primary epidermal keratinocytes were isolated from respective wild type and Snail transgenic B6J-2019 mouse strains and cultured as described previously(*29*). The keratinocytes were grown in low calcium (50uM) E-media. For differentiation assay, E-media containing 1.2mM calcium was used and kept for indicated time points.

Antibodies and Reagents

The following antibodies were used in the study: p-STAT3 (9145S-CST), STAT3 (4904-CST), GAPDH (ab8245-abcam), p-Src (2101-CST), Src (2123-CST), CD11b (14-0112-82-eBiosciences for immunofluorescence and immunoprecipitation, 50-161-42-Invitrogen™ for flow cytometry and PA5-90724-Invitrogen for western blot) , RatIgG isotype control (12-432180-Invitrogen), EEA1 (BD610456 BD biosciences), F-Spondin (HPA066095-Sigma), CD44 (550538-BD).
The following reagents were used: Hoechst (H3570-Life Technologies), Dynasore (D7693-Sigma-Aldrich), Src inhibitor (4660-Tocris).

Protein purification

The cDNA encoding the F-Spondin domain of Mindin was cloned into a pET-28a expression vector with an N-terminal 6×His tag and transformed into *E. coli* BL21 (DE3) competent cells. A single colony was inoculated into LB medium supplemented with kanamycin and grown overnight at 37 °C. The overnight culture was diluted 1:100 into fresh LB medium and grown at 37 °C until OD_{600} reached 0.6–0.8, followed by induction with 250 mM IPTG at 18 °C for 10-12 hrs with constant shaking at 180rpm.
Cells were harvested by centrifugation (5000 × g, 15 min, 4 °C), resuspended in lysis buffer (20 mM Tris-HCl pH 8.0, 300 mM NaCl, 10 mM imidazole, 1 mM PMSF), and lysed by sonication on ice. The lysate was clarified by centrifugation at 15,000 × g for 45 min at 4 °C, and the supernatant was loaded onto Ni-NTA column (Biorad) pre-equilibrated with lysis buffer. The resin was washed extensively with wash buffer (20 mM Tris-HCl pH 8.0, 300 mM NaCl, 30–40 mM imidazole) to remove non-specifically bound proteins, and bound proteins were eluted using elution buffer (20 mM Tris-HCl pH 8.0, 300 mM NaCl, 100-250 mM imidazole).

The eluted protein was concentrated using Amicon Ultra centrifugal filters (Millipore, 3 kDa cutoff) and subjected to size-exclusion chromatography (SEC) on a Superdex 200 Increase 10/300 GL column (Cytiva) pre-equilibrated with SEC buffer (10 mM Tris-HCl pH 8.0, 20 mM NaCl) using an ÄKTA pure system. Peak fractions corresponding to the target protein were pooled and concentrated. Protein purity was assessed by SDS–PAGE followed by Silver-nitrate staining, and concentrations were determined using nano-drop. The purified F-Spondin was used at a concentration of 250ng/ml in all treatments. All treatments were done in serum-free conditions unless otherwise stated.

Histidine-tagged Mindin was purified from conditioned media collected from Mindin expressing Chinese hamster ovary cells using Ni-NTA column. Buffers with varying strengths of imidazole were made in 20 mM Tris and 300 mM NaCl (pH = 8) for washing and elution. The purified Mindin (10 mL) was dialyzed for 3 rounds in 1 L dialysis buffer (10 mM tris, 20 mM NaCl, pH = 8), concentrated using a 10 kDa Centricon concentrator, and filtered with a 0.2 µm syringe filter. Silver staining was performed to assess the purity and confirm the purification of Mindin. The purified recombinant Mindin was used at a concentration of 80–200 ng/mL in all treatments. All treatments were done in serum-free conditions unless otherwise stated.

Western Blotting

Keratinocyte lysates were prepared in RIPA buffer (50 mM Tris-HCl, pH 7.4; 150 mM NaCl; 1% NP-40; 0.1% SDS; 0.5% sodium deoxycholate) supplemented with protease (S8830, Sigma) and phosphatase (04 906 837 001, Roche) inhibitors and sonicated on ice at 4 °C. Equal amounts of protein were mixed with 4× Laemmli sample buffer, boiled at 95 °C for 3 min, and resolved by SDS–PAGE. Proteins were transferred onto nitrocellulose membranes using a wet transfer system. Membranes were blocked for 1 h at room temperature with either 5% BSA in Tris-buffered saline containing 0.1% Tween-20 (TBST) for phosphorylated proteins, or 5% Blotto (Santa Cruz Biotechnology, sc-2325) for total proteins. Membranes were then incubated overnight at 4 °C with the appropriate primary antibodies, followed by HRP-conjugated secondary antibodies for 1 h at room temperature. After extensive washing with TBST, signals were detected using enhanced chemiluminescence (ECL, Merck) and visualized on an iBright FL (Thermo Fisher) imaging system. Band intensities were quantified using Fiji (ImageJ), and values were normalized to the respective loading controls.

Gene expression

Total RNA was extracted from keratinocytes using RNAIso Plus (9109-Takara) according to the manufacturer's instructions. RNA purity and concentration were assessed using a NanoDrop spectrophotometer and RNA integrity was verified by agarose gel electrophoresis. For cDNA synthesis, 2 µg of total RNA was reverse transcribed using the PrimeScript™ RT Reagent Kit (Perfect Real Time, RR037A, Takara) following the recommended protocol.

Quantitative real-time PCR (qRT-PCR) was performed using TB Green® Premix Ex Taq™ II (Tli RNaseH Plus, RR820A, Takara). Each reaction was run in triplicate, and relative gene expression was calculated using the 2^(-ΔΔCt) method, normalized to TBP as the endogenous control.

Following is the list of primer pairs used for gene expression analysis:

Myc: Fwd-CCTCACTCCTAATCCGGTCAT
Rvs-GTGCTGTAGTTTTTCGTTCACTG

CyclinD1: Fwd- GCGTACCCTGACACCAATCTC
Rvs- CTCCTCTTCGCACTTCTGCTC

Sox4: Fwd-GACAGCGACAAGATTCCGTTC
Rvs-GTTGCCCGACTTCACCTTC

IGIF1R: Fwd-GTGGGGGCTCGTGTTTCTC
Rvs-GATCACCGTGCAGTTTTCCA

TBP: Fwd-AGTGCCGCCCAAGTAGCA
Rvs-TCCCCCTCTGCACGTAAATC

Immunoprecipitation

Keratinocytes were lysed in ice-cold lysis buffer (50 mM Tris-HCl, pH 7.4; 150 mM NaCl; 1% NP-40) supplemented with protease (S8830, Sigma) and phosphatase (04 906 837 001, Roche) inhibitors. For each reaction, equal amounts of protein were incubated overnight at 4 °C with the indicated primary antibody or isotype control IgG. Antibody–protein complexes were captured by incubation with Protein G agarose beads (Thermo Fisher Scientific) for 30 mins. at room temperature with gentle rotation. Beads were washed three times with lysis buffer, and bound proteins were eluted by boiling in 2× Laemmli sample buffer for 10 min at 95 °C. Eluates were resolved by SDS–PAGE and analyzed by immunoblotting with the respective antibodies.

Immunostaining and image acquisition

Primary mouse keratinocytes were seeded on 10 mm circular coverslips coated with Rat tail Type-I collagen (50 ug/ml, Gibco- A1048301). At the end of the experiments, cells on coverslips were washed and fixed using 4%Paraformaldehyde at 25^0C for 10 mins. The cells were then permeabilized using 0.2% Triton-X100 at 25^0C for 10 mins. The cells were blocked using 5% BSA blocking solution in TBST for 30-60 mins. This was followed by primary antibody staining overnight at 4^0C. The next day, primary antibody was removed followed by three washes with TBST, 10 mins. each. Cells on coverslip were then incubated with respective secondary antibodies and Hoechst (to stain the nucleus) for 30 mins. – 1 hour followed by three washes TBST for 5-7 min. each and mounted with Mowiol 4-88 (81381-50G, Sigma-Aldrich).

The images were acquired using an Olympus FV3000 confocal microscope and processed using FIJI software. Z-stack images were obtained at a resolution of 800 × 800 pixels and were subsequently visualized and generated using FIJI software.

Colocalisation analysis

For co-localization of CD11b and EEA1, cells were imaged using a (Olympus FV3000 confocal microscope with PLAPON 60X objective having a 1.42 numerical aperture, oil immersion, and a 1 µm pinhole setting). Images were acquired as z-stacks with an optical section thickness of ~0.3 µm to capture the full cellular volume. Co-localization analysis was performed on single optical sections to avoid artifacts from projected planes. Background fluorescence was subtracted uniformly from all channels prior to analysis. Individual cells were selected as regions of interest (ROIs) to exclude adjacent cells or extracellular signals. The degree of co-localization was quantified using the Pearson's correlation coefficient, measured with the *Coloc2* plug-in in FIJI (ImageJ). Identical thresholding parameters were applied across datasets to minimize bias. Pearson's coefficients were calculated per ROI, and values from individual cells were plotted as single data points in the graphs. At least n = 30 cells from 3 independent experiments were analyzed per condition.

Flow Cytometry

Keratinocytes were harvested using EDTA solution and washed twice with ice-cold PBS containing 1% FBS (FACS buffer). For surface staining, 1×10^6 cells were resuspended in FACS

buffer and incubated with CD11b Monoclonal Antibody (M1/70), APC-eFluor™ 780 for 30 mins on ice washed twice in FACS buffer and resuspended in 500 µLFACS buffer. Data were acquired on the Attune NxT Acoustic Focusing Cytometer (Invitrogen).

Transcriptome analysis (RNA-seq) using RNAlysis

Raw FASTQ files were imported into RNAlysis (3.9.2) Kallisto Paired-end RNA-seq quantification tool under FASTQ tab. The count matrix file from Kallisto quantification was imported for DESeq2 normalisation within RNAlysis. Low-abundance genes were filtered. Genes were called differentially expressed (DEGs) at adjusted p-values< 0.05 and $|\log2 \text{ fold-change}| \geq 1$, unless otherwise indicated.

Lists of up-regulated and down-regulated DEGs (separately) were submitted to DAVID Bioinformatics Resources (v2023q4; build noted at submission). Enrichment was assessed for GOTERM_BP_DIRECT. Terms with adjusted p-value<0.05 were considered significant. Statistics were taken directly from DAVID.

Overlaps among DEG sets from Mindin and F-Spondin comparisons were computed on gene symbols. Venn diagrams were generated with Venny 2.0 using the exact DEG lists and thresholds defined above.

Nuclear to Cytoplasmic ratio

Keratinocytes were cultured on coverslips, fixed with 4% paraformaldehyde (PFA) for 10 min at room temperature, permeabilized using 0.2% Triton X-100 in PBS, and stained with Hoechst (for nuclei) and phalloidin–Alexa Fluor 568 to delineate cell boundaries. Confocal z-stacks were acquired using a (Olympus FV3000 confocal microscope) under identical acquisition parameters for all conditions.

Image processing: Images were analyzed using FIJI (ImageJ). Nuclear ROIs were generated by automatic thresholding of the DAPI channel, followed by manual curation to exclude overlapping or fragmented nuclei. Cytoplasmic area was calculated from subtracting nuclear area from total cell area generated from phalloidin/cytoplasmic marker-defined cell boundary. The nuclear and cytoplasmic areas were computed from the segmented ROIs. The ratio was calculated as: N/C ratio (area)= Nuclear area/Cytoplasmic area

Colony forming assay

Keratinocytes were seeded at a low density (1,000 cells per well) in 6-well culture plates and allowed to adhere for 12 hours. After 12 hours Mindin/F-Spondin treatment was initiated and supplemented every alternate day. The cells were maintained under standard growth conditions in DMEM-F12 and 1XPen-Strep solution (A001A-100ML-HiMedia) for 10–14 days without disturbance, allowing colonies to form. At the end of the incubation period, colonies were washed gently with PBS, fixed with 4% paraformaldehyde for 15 min, and stained with 0.5% crystal violet solution in 25% methanol for 30 min. Excess stain was removed by washing with distilled water, and plates were air-dried. Colonies containing more than 10 cells were counted manually using a light microscope or automatically using FIJI (ImageJ) software.

Author contributions

Conceptualization: BD, KB, CJ; Methodology: BD, KB, JA, TS, AH, SK, CJ; Investigation: BD, JA, TS, AH, AD, SJ, SK; Formal Analysis: BD, JA, TS, AH, AD; Visualization: BD, JA; Funding Acquisition: CJ; Supervision: CJ; Writing - Original Draft Preparation: BD, KB, CJ; Writing - Review and Editing: BD, CJ.

Acknowledgments

The authors would like to thank members of the Jamora laboratory for critical review of the manuscript. We would like to thank Akanksha Srivastava for generating the F-Spondin clone. This work was supported by core funds from inStem and Shiv Nadar Institution of Eminence and by grants from the Department of Biotechnology of the Government of India (BT/PR8738/AGR/36/770/2013 and BT/PR32539/BRB/10/1814/2019) and the Indian Council of Medical Research (IIRPIG-2024-01-01387). Animals are maintained at the BLiSC Animal Care and Resource Center (ACRC) and is partially supported by the National Mouse Research Resource grant BT/ PR5981/MED/31/181/2012;2013-2016;2018 and 102/IFD/SAN/5003/2017-2018 from the Department of Biotechnology.

Conflict of interest: The authors have declared that no conflict of interest exists.

Reference

1. E. Rognoni, F. M. Watt, Skin Cell Heterogeneity in Development, Wound Healing, and Cancer. *Trends Cell Biol.* **28**, 709 (2018).
2. T. T. Q. Pham, Y. C. Kuo, W. L. Chang, H. J. Weng, Y. H. Huang, Double-sided niche regulation in skin stem cell and cancer: mechanisms and clinical applications. *Mol. Cancer 2025 241* **24**, 1–61 (2025).
3. C. D. Mohan, S. Rangappa, H. D. Preetham, S. Chandra Nayaka, V. K. Gupta, S. Basappa, G. Sethi, K. S. Rangappa, Targeting STAT3 signaling pathway in cancer by agents derived from Mother Nature. *Semin. Cancer Biol.* **80**, 157–182 (2022).
4. D. J. Jonker, L. Nott, T. Yoshino, S. Gill, J. Shapiro, A. Ohtsu, J. Zalcberg, M. M. Vickers, A. C. Wei, Y. Gao, N. C. Tebbutt, B. Markman, T. Price, T. Esaki, S. Koski, M. Hitron, W. Li, Y. Li, N. M. Magoski, C. J. Li, J. Simes, D. Tu, C. J. O'Callaghan, Napabucasin versus placebo in refractory advanced colorectal cancer: a randomised phase 3 trial. *Lancet Gastroenterol. Hepatol.* **3**, 263–270 (2018).
5. P. Yue, J. Turkson, Targeting STAT3 in cancer: how successful are we? doi: 10.1517/13543780802565791.
6. K. Badarinath, B. Dam, Y.-W. He, S. Krishna, C. Jamora, S. Kataria, R. K. Zirmire, R. Dey, G. Kansagara, J. Ajnabi, A. Hegde, R. Singh, T. Masudi, J. Sambath, S. P. Sachithanandan, P. Kumar, A. Gulyani, Snail maintains the stem/progenitor state of skin epithelial cells and carcinomas through the autocrine effect of matricellular protein Mindin. *CellReports* **40**, 111390 (2022).
7. M. von Zastrow, A. Sorkin, Signaling on the endocytic pathway. *Curr. Opin. Cell Biol.* **19**, 436 (2007).
8. M. Miaczynska, D. Bar-Sagi, SIGNALING ENDOSOMES: SEEING IS BELIEVING. *Curr. Opin. Cell Biol.* **22**, 535 (2010).
9. Y. Li, C. Cao, W. Jia, L. Yu, M. Mo, Q. Wang, Y. Huang, J.-M. Lim, M. Ishihara, L. Wells, P. Azadi, H. Robinson, Y.-W. He, L. Zhang, R. A. Mariuzza, Structure of the F-spondin domain of mindin, an integrin ligand and pattern recognition molecule. *EMBO J.* **28**, 286–297 (2009).
10. Y. sheng Liu, L. fen Wang, X. S. Cheng, Y. N. Huo, X. M. Ouyang, L. Y. Liang, Y. Lin, J. F. Wu, J. L. Ren, B. Guleng, The pattern-recognition molecule mindin binds integrin

Mac-1 to promote macrophage phagocytosis via Syk activation and NF-κB p65 translocation. *J. Cell. Mol. Med.* **23**, 3402–3416 (2019).

11. A. Sorkin, M. Von Zastrow, N. Rev, Endocytosis and signalling: intertwining molecular networks. *Nat Rev Mol Cell Biol* **10**, 609–622 (2010).
12. S. Ahn, J. Kim, C. L. Lucaveche, M. C. Reedy, L. M. Luttrell, R. J. Lefkowitz, Y. Daaka, Src-dependent Tyrosine Phosphorylation Regulates Dynamin Self-assembly and Ligand-induced Endocytosis of the Epidermal Growth Factor Receptor. *J. Biol. Chem.* **277**, 26642–26651 (2002).
13. D. Fessart, M. Simaan, S. A. phane Laporte, c-Src Regulates Clathrin Adapter Protein 2 Interaction with-Arrestin and the Angiotensin II Type 1 Receptor during Clathrin-Mediated Internalization. doi: 10.1210/me.2004-0246 (2005).
14. J. Huynh, A. Chand, D. Gough, M. Ernst, Therapeutically exploiting STAT3 activity in cancer — using tissue repair as a road map. *Nat. Rev. Cancer 2018 192* **19**, 82–96 (2018).
15. M. M. Sherry, A. Reeves, J. K. Wu, B. H. Cochran, STAT3 Is Required for Proliferation and Maintenance of Multipotency in Glioblastoma Stem Cells. *Stem Cells* **27**, 2383–2392 (2009).
16. L. Hanousková, J. Řezá~, [Těpán Veselý, R. Prů{a, K. Kota{ka, DIAGNOSTIC BENEFITS OF MINDIN AS A PROSTATE CANCER BIOMARKER DIJAGNOSTI^KE PREDNOSTI MINDINA KAO BIOMARKERA RAKA PROSTATE. *J Med Biochem* **39**, 108–111 (2020).
17. M. A. Alfonzo-Méndez, K. A. Sochacki, M. P. Strub, J. W. Taraska, Dual clathrin and integrin signaling systems regulate growth factor receptor activation. *Nat. Commun. 2022 131* **13**, 1–16 (2022).
18. A. Elbediwy, Z. I. Vincent-Mistiaen, B. Spencer-Dene, R. K. Stone, S. Boeing, S. K. Wculek, J. Cordero, E. H. Tan, R. Ridgway, V. G. Brunton, E. Sahai, H. Gerhardt, A. Behrens, I. Malanchi, O. J. Sansom, B. J. Thompson, Integrin signalling regulates YAP and TAZ to control skin homeostasis. *Dev.* **143**, 1674–1687 (2016).
19. N. R. Paul, G. Jacquemet, P. T. Caswell, Endocytic Trafficking of Integrins in Cell Migration. *Curr. Biol.* **25**, R1092–R1105 (2015).
20. J. L. Stow, P. Lacy, H. Warner, D. Schmidt-Arras, S. Rose-John, Endosomes as Signaling Platforms for IL-6 Family Cytokine Receptors. doi: 10.3389/fcell.2021.688314 (2021).

21. C. L. German, C. L. Howe, The STAT3 Beacon: Signal Transducer and Activator of Transcription 3 is Activated and Transcriptionally Regulated by Endosomal Structures. *Exp Cell Res* **317**, 1955–1969 (2011).
22. A. Sinha, R. J. Khadilkar, K. S. Vinay, A. R. Sinha, Europe PMC Funders Group Conserved Regulation of the JAK / STAT Pathway by the Endosomal Protein Asrij Maintains Stem Cell Potency. **4**, 649–658 (2015).
23. A. Foster-Barber, J. M. Bishop, Src interacts with dynamin and synapsin in neuronal cells. *Proc. Natl. Acad. Sci. U. S. A.* **95**, 4673–4677 (1998).
24. A. Wilde, E. C. Beattie, L. Lem, D. A. Riethof, S.-H. Liu, W. C. Mobley, P. Soriano, F. M. Brodsky, EGF Receptor Signaling Stimulates SRC Kinase Phosphorylation of Clathrin, Influencing Clathrin Redistribution and EGF Uptake. *Cell* **96**, 677–687 (1999).
25. T. Stasyk, L. A. Huber, Spatio-Temporal Parameters of Endosomal Signaling in Cancer: Implications for New Treatment Options. *J. Cell. Biochem.* **117**, 836 (2015).
26. M. A. Dozynkiewicz, N. B. Jamieson, I. Macpherson, J. Grindlay, P. V. E. Van Den Berghe, A. Von Thun, J. P. Morton, C. Gourley, P. Timpson, C. Nixon, C. J. Mckay, R. Carter, D. Strachan, K. Anderson, O. J. Sansom, P. T. Caswell, J. C. Norman, Article Rab25 and CLIC3 Collaborate to Promote Integrin Recycling from Late Endosomes / Lysosomes and Drive Cancer Progression. *Dev. Cell* **22**, 131–145 (2012).
27. H. Ying, H. Zheng, K. Scott, R. Wiedemeyer, H. Yan, C. Lim, J. Huang, Mig-6 controls EGFR traf fi cking and suppresses gliomagenesis. **107**, 6–11 (2010).
28. Y. Y. Lee, H. K. Jeon, J. Lee, J. E. Hong, I. G. Do, C. H. Choi, T. J. Kim, B. G. Kim, D. S. Bae, Y. C. Kim, J. W. Lee, Dynamin 2 inhibitors as novel therapeutic agents against cervical cancer cells. *Anticancer Res.* **36**, 6381–6388 (2016).
29. E. Nowak, J.A., Fuchs, Isolation and Culture of Epithelial Stem Cells. *Methods Mol. Biol.*, doi: https://doi.org/10.1007/978-1-59745-060-7_14.